Active Particles with Soft and Curved Walls: Equation of State, Ratchets, and Instabilities

Nikolai Nikola,[1] Alexandre P. Solon,[2,3] Yariv Kafri,[1] Mehran Kardar,[3] Julien Tailleur,[2] and Raphaël Voituriez[4,5]
[1]*Department of Physics, Technion, Haifa 32000, Israel*
[2]*Université Paris Diderot, Sorbonne Paris Cité, MSC, UMR 7057 CNRS, 75205 Paris, France*
[3]*Department of Physics, Massachusetts Institute of Technology, Cambridge, Massachusetts 02139, USA*
[4]*Laboratoire de Physique Théorique de la Matière Condensée, UMR 7600 CNRS /UPMC, 4 Place Jussieu, 75255 Paris Cedex, France*
[5]*Laboratoire Jean Perrin, UMR 8237 CNRS /UPMC, 4 Place Jussieu, 75255 Paris Cedex, France*
(Received 17 December 2015; revised manuscript received 10 May 2016; published 22 August 2016)

We study, from first principles, the pressure exerted by an active fluid of spherical particles on general boundaries in two dimensions. We show that, despite the nonuniform pressure along curved walls, an equation of state is recovered upon a proper spatial averaging. This holds even in the presence of pairwise interactions between particles or when asymmetric walls induce ratchet currents, which are accompanied by spontaneous shear stresses on the walls. For flexible obstacles, the pressure inhomogeneities lead to a modulational instability as well as to the spontaneous motion of short semiflexible filaments. Finally, we relate the force exerted on objects immersed in active baths to the particle flux they generate around them.

DOI: 10.1103/PhysRevLett.117.098001

Active forces have recently attracted much interest in many different contexts [1]. In biology, they play crucial roles on scales ranging from the microscopic, where they control cell shape and motion [2], to the macroscopic, where they play a dominant role in tissue dynamics [3,4]. More generally, active systems offer novel engineering perspectives, beyond those of equilibrium systems. In particular, boundaries have been shown to be efficient tools for manipulating active particles. Examples range from the rectification of bacterial densities [5,6] and optimal delivery of passive cargoes [7] to the powering of microscopic gears [8,9]. Further progress, however, requires a predictive theoretical framework which is currently lacking for active systems. To this end, simple settings have been at the core of recent active matter research.

Understanding the effect of boundaries on active matter starts with the mechanical pressure exerted by an active fluid on its containing vessel. This question has been recently studied extensively for dry systems [10–17], revealing a surprisingly complex physics. For generic active fluids, the mechanical pressure is *not* a state variable [13]. The lack of an equation of state, through a dependence on the wall details, questions the role of the mechanical pressure in any possible thermodynamic description of active systems [18,19]; it also leads to a richer phenomenology than in passive systems by allowing more general mechanical interplays between fluids and their containers.

Interestingly, for the canonical model of self-propelled spheres with constant propelling forces, on which neither walls nor other particles exert torques, the pressure acting on a *solid flat* wall has been shown to admit an equation of state [11,12,19]. While the physics of this model does not clearly differ from other active systems, showing, for instance, wall accumulation [20] and motility-induced phase separation [21–23], the mechanical pressure exerted on a flat wall satisfies an equation of state even in the presence of pairwise interactions [11,12,19]. One might thus hope that the intuition built on the rheology of equilibrium fluids extends to this case. Derived in a particular setting, the robustness of this equation of state, however, remains an open question. For instance, the physics of active fluids near curved and flat boundaries is very different [10,14,15,24,25]. Specifically, particles accumulate nonevenly depending on the curvature of confining walls, generating a spatially varying pressure [24,25]. Furthermore, the interplay between active particles and flexible objects, such as polymers and membranes, shows a rich nonequilibrium phenomenology [26–34]. Characterizing the role and properties of active forces in these contexts is thus an open and challenging question.

In this Letter, we study, from first principles, the confinement of torque-free active particles beyond the case of solid flat walls. We first show analytically that, while the pressure on curved walls is inhomogeneous, one recovers an equation of state for the average force *normal* to the wall, even in the presence of pairwise interactions. This surprising result also holds for asymmetric walls which act as ratchets and, as we show, generate currents and forces tangential to the wall. Contrary to the average normal force, these shear stresses depend on the details of the potential used to model the wall and therefore do not admit an equation of state. Moreover, we show that the pressure inhomogeneities trigger interesting new physics. For flexible partitions, we show how a finite-wavelength modulational instability sets in, followed by a long-time coarsening. Interestingly, this also explains the atypical folding and self-propulsion of semiflexible filaments immersed in active baths [28,30]. Finally, we give a simple

relation between the force exerted on an asymmetric object in an active bath and the current of active particles it generates around it.

We start by considering noninteracting active particles, of positions $\mathbf{r}_i = (x_i, y_i)$ and headings $\mathbf{e}_{\theta_i} = (\cos\theta_i, \sin\theta_i)$, which follow the Langevin equations

$$\dot{\mathbf{r}}_i = v\mathbf{e}_{\theta_i} - \mu_t \boldsymbol{\nabla} V + \sqrt{2D_t}\boldsymbol{\eta}_i(t), \tag{1}$$

$$\dot{\theta}_i = \sqrt{2D_r}\eta_i^r(t) \tag{2}$$

in addition to randomly changing orientation (tumbling) with rate α. Here v is the propulsion speed, μ_t is the translational mobility [35], D_t and D_r are the translational and rotational diffusivities, respectively, $V(\mathbf{r})$ is a static potential which defines the confining walls, and the η's are unit-variance Gaussian white noises. This model encompasses the well-studied run-and-tumble (RTP) dynamics and active Brownian particles (ABPs), with pure rotational diffusion. The persistence length of the particle, or run length, is given by $v/(D_r + \alpha)$.

We first consider a system with periodic boundary conditions along the $\hat{y}$ direction and structured walls along the $\hat{x}$ direction. The wall potential starts, say, along the right edge of the system, at $x_w(y) = x_0 + A\sin(2\pi y/L_p)$, and takes the form $V(\mathbf{r}) = \frac{1}{2}\lambda[x - x_w(y)]^2$ for $x > x_w$, with a mirrored opposing wall at $-x_w(y)$. The system height in the $\hat{y}$ direction is taken to be an integer times L_p. Equations of state, in or out of equilibrium, exist only in the thermodynamic limit, and we always take the distance between the walls much larger than any correlation length. The bulk is then uniform, isotropic, and independent of what happens in the boundary layers close to the walls; we thus consider only one edge of the system.

Let us first consider *hard* walls, with λ large enough that particles are arrested by the wall potential on a scale orders of magnitude smaller than any other relevant length scales. Examples of numerically measured steady-state particle and current densities are shown in Figs. 1(a) and 1(b). As expected [14,24,25], the density along and close to the wall is nonuniform and, in general, unequal at points of equal potential (as opposed to what happens at thermal equilibrium). Remarkably, in addition to the thin layer close to the wall where particles accumulate, complex potential-dependent steady-state densities and currents are found in the whole wall region. There is a depletion of particles in the *outer concave* region of the wall, where particles stream towards the outer apices, and a density increase close to the *inner convex* apices, due to the recirculation of particles along the walls. Most importantly, the local pressure varies considerably along the wall [36] [see Fig. 1(d)]. For hard walls, the force is always normal to the wall surface, and the local pressure can be evaluated as $P(y) = \int_{\mathbf{r}_\star}^{\infty} \rho(\mathbf{r})\boldsymbol{\nabla} V \cdot d\mathbf{r}$, where the integral is taken in the direction normal to the wall, $\mathbf{r}_\star$ is inside the bulk of the system, and $\rho(\mathbf{r})$ is the density of particles. Somewhat counterintuitively, the pressure is highest close to the depleted region, at the outer apices, because

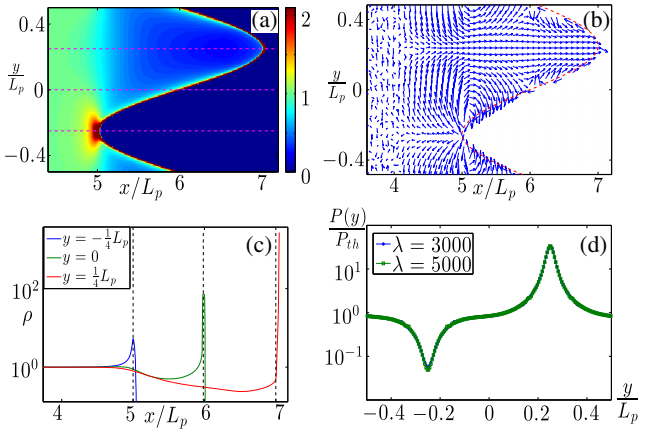

FIG. 1. The density (a) and current (b) of noninteracting ABPs near the right edge of the system with the hard wall potential described in the text with $v = D_r = 24$, $D_t = 0$, $L_p = 0.5$, $A = 0.5$, and $\lambda = 1000$. The red dashed curve corresponds to $x_w(y)$. (c) Three cross sections of the particle density taken at the three horizontal dashed lines in (a). The vertical lines correspond to $x_w(y)$. (d) Pressure normal to the wall, normalized by Eq. (6), as a function of y, in the hard wall regime.

the depletion is compensated by a stronger accumulation at the wall, where the potential is nonzero [see Fig. 1(c)]. Similarly, it is lowest at regions where there is an accumulation of particles near the wall. Finally, we find, numerically, that the ratio between the maximal and minimal pressures (at the outer and inner apices, respectively) is a function of the dimensionless parameter $v/(D_r R)$ [Fig. 2(b)], where $R = L_p^2/(4\pi^2 A)$ is the radius of curvature at the apices.

Naively, these results suggest that the equation of state obtained in Ref. [13] for this model is valid only for flat walls. However, Fig. 2 shows that the pressure, despite its nonuniformity, satisfies the same equation of state as in the case of flat walls [13] once averaged over a period of the wall. More precisely, the force per unit length acting on a period of the potential, defined as

$$\langle P_x \rangle = \frac{1}{L_p}\int_0^{L_p} P_x(y)dy, \qquad P_x(y) = \int_{x_\star}^{\infty} \rho(\mathbf{r})\partial_x V dx \tag{3}$$

with $P_x(y)$ the force per unit length exerted by active particles on the wall along the $\hat{x}$ direction [37], obeys an equation of state. (By symmetry, for the potentials considered so far, the mean force along the $\hat{y}$ direction is zero.) The averaged pressure is thus independent of the wall potential, whether hard or soft, a result which persists for any $V(\mathbf{r})$ despite the fact that the local pressure depends on the exact form of the wall potential [38]. It would be interesting to see if this can be related to the applicability of the virial theorem to the systems we consider here [11,12,16,17,39].

To prove this result, consider the dynamics of the probability density to find a particle at $\mathbf{r}$ with orientation θ:

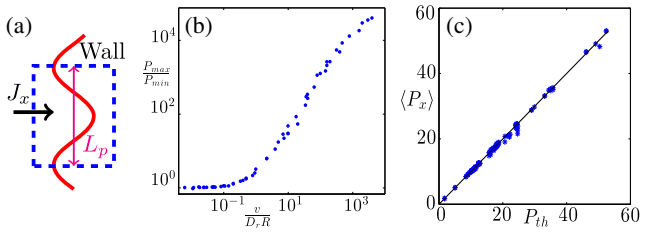

FIG. 2. (a) For a periodic wall, the probability flux is periodic along y and vanishes in the wall so that $\int_0^{L_p} J_x dy = 0$ in steady state. (b) The ratio between the maximal and minimal values of $P_x(y)$ on hard sinusoidal walls as a function of $v/D_r R$, where $R = L_p^2/(4\pi^2 A)$ is the radius of curvature, measured for a variety of combinations with $v \in [0.05, 40]$, $A \in [0.3, 12]$, $D_r \in [0.1, 20]$, $L_p \in [0.3, 80]$, and $\lambda = 1000$–3000. (c) Mean pressure versus its theoretical prediction Eq. (6). Data were collected from 70 simulations of ABPs, RTPs, passive Brownian particles, and combinations thereof, with symmetric and asymmetric, hard and soft, periodic walls.

$$\partial_t \mathcal{P}(\mathbf{r},\theta) = -\boldsymbol{\nabla}\cdot(v\mathbf{e}_\theta - \mu_t \boldsymbol{\nabla} V - D_t \boldsymbol{\nabla})\mathcal{P}(\mathbf{r},\theta) + (D_r \partial_\theta^2 - \alpha)\mathcal{P}(\mathbf{r},\theta) + \frac{\alpha}{2\pi}\int_0^{2\pi} d\theta' \mathcal{P}(\mathbf{r},\theta'). \tag{4}$$

Integrating over θ yields in steady state $\nabla \cdot \mathbf{J} = 0$, where

$$\mathbf{J}(\mathbf{r}) = v\int_0^{2\pi} \mathbf{e}_\theta \mathcal{P} d\theta - \mu_t \tilde{\rho} \nabla V - D_t \nabla \tilde{\rho} \tag{5}$$

and $\tilde{\rho}(\mathbf{r}) = \int d\theta \mathcal{P}(\mathbf{r},\theta)$. For flat walls, the invariance along $\hat{y}$ of the system imposes $J_x = 0$, which directly leads to an equation of state for the local force per unit length in the $\hat{x}$ direction [13]. While J_x can be locally nonzero for structured walls, the mean flux of particles through a closed path still has to vanish in steady state. It is then always possible to find a length L_p such that $\int_0^{L_p} dy J_x(x,y) = 0$, where L_p can, for instance, be the period of a periodic potential or the full wall length [see Fig. 2(a)]. Following Ref. [13], one can then construct an equation of state for $\langle P_x \rangle$ instead of the local pressure P_x. For instance, for noninteracting particles,

$$\langle P_x \rangle = \rho_0 \left[\frac{v^2}{2\mu_t(D_r+\alpha)} + \frac{D_t}{\mu_t}\right] \equiv P_{th} \tag{6}$$

perfectly fits our simulations (see Fig. 2), where ρ_0 is the mean number density of particles in the bulk. The full proof, allowing for pairwise interactions, is given in Ref. [38].

Interestingly, the equation of state is valid for any wall, including asymmetric ones which, in the spirit of ratchets [5,40–43], may induce a net particle current along the wall. Such a current, whose direction can be controlled by the asymmetry of the wall, is accompanied by a shear force exerted by the active particles on the wall, parallel to its general surface. This is illustrated in Fig. 3 for an asymmetric wall potential given by

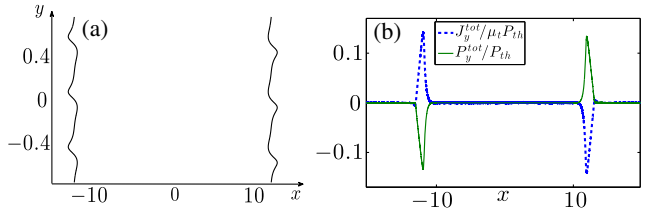

FIG. 3. (a) Equipotential line ($V = 5$) of the asymmetric potential (7). (b) Ratchet current and shear stress as functions of x. Equation (9) is verified numerically within 1%. Simulation of ABPs with $x_0 = 10$, $\lambda = 2$, $A = 0.3$, $L_p = 0.5$, and $v = D_r = 24$.

$$V(x,y) = \frac{1}{2}\lambda(x-x_0)^2\left[1 + A e^{\cos(2\pi y/L_p)} \sin\left(\frac{2\pi y}{L_p}\right)\right]. \tag{7}$$

This spontaneous shear stress exerted by an active fluid on an asymmetric surface is impossible in equilibrium systems. It can be quantified as (see Fig. 3)

$$P_y^{\mathrm{tot}}(x) = \int_0^{L_p} dy \rho(\mathbf{r}) \partial_y V(\mathbf{r}). \tag{8}$$

This explains the spontaneous rotation of microscopic gears [8,9] and relates to the ratchet current through

$$\int_{x_\star}^{\infty} dx P_y^{\mathrm{tot}} = -\frac{1}{\mu_t}\int_{x_\star}^{\infty} dx J_y^{\mathrm{tot}}. \tag{9}$$

Here $J_y^{\mathrm{tot}}(x) = \int_0^{L_p} J_y(\mathbf{r}) dy$ is the total current in the $\hat{y}$ direction (see Ref. [38] and Fig. 3), and Eq. (9) is the total force exerted by the active fluid on one period of the wall in the $\hat{y}$ direction. Note that $\langle P_x \rangle$, despite all these complications, still satisfies the same equation of state as for symmetric walls.

As shown above, although the averaged pressure satisfies an equation of state, the details of the interaction with the wall, e.g., the local pressure, are quite unlike an equilibrium system. Specifically, we note that, for hard surfaces, the highest pressure is always at the concave apex of the wall surface, while the lowest pressure is at the convex apex. We now show that for flexible objects this leads to a generic modulational instability.

The origin of the instability can be understood by considering a flexible interface (a filament in 2D), characterized by stretching and bending rigidities and anchored at the top and bottom of a container holding the active particles (see Fig. 4). The results above imply that, once induced by a fluctuation, a local deformation will have a finite pressure difference on the two sides of its apices, which will tend to further increase the deformation. Within linear stability analysis, the fate of a fluctuation of wave number q can be understood as follows: The unstabilizing contribution of the active pressure scales as the curvature of the interface (see Fig. 2 and Ref. [38]) and, hence, as q^2. It competes with the stabilizing effects of the tension and the

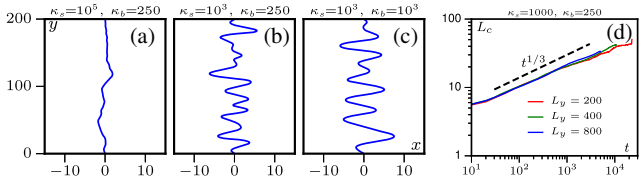

FIG. 4. Snapshots of a flexible interface in an active bath, not shown for clarity. The stretching constant controls the threshold (a),(b) while the bending constant controls the wavelength of the instability (b),(c). Snapshots were taken at $t = 30$ after starting from a straight filament. The characteristic length L_c, defined as the first zero of the autocorrelation function of the transverse monomer displacement, slowly coarsens as time goes on (d). Parameters are $\rho_0 = 1$, $v = 10$, $D_r = 1$, $r_1 = r_0 = 0.3$, $\kappa_s = 1000$, and $\kappa_b = 250$.

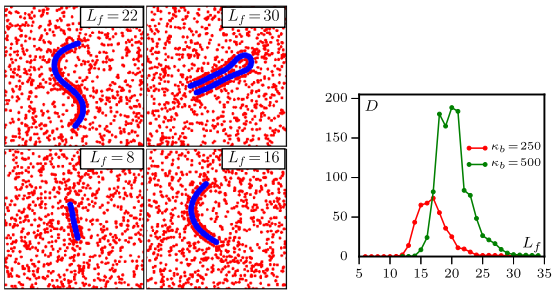

FIG. 5. (Left) Typical configurations for filaments of varying length for $\kappa_b = 250$, $v = 10$, $D_r = 1$, $\rho_0 = 1$, $\kappa_s = 1000$, $r_1 = r_0 = 0.3$, and box size 50×50 with periodic boundary conditions. (Right) Diffusivity of the filament as a function of its length.

bending rigidities, which scale as q^2 and q^4, respectively. This implies that, for large enough activity, the interface is unstable below a certain wave number q_c with a fastest growing mode $q_{\max}$ controlled by the interplay between the tension, activity, and the bending rigidity. (See Ref. [38] for details and estimates of q_c.)

To observe the instability, we carried out numerical simulations (videos provided in Ref. [38]), in which a semiflexible filament with fixed ends is immersed in an active gas of ABPs. The filament is modeled as a chain of beads whose potential energy is given by

$$E = \sum_{i=1}^{N-1} \frac{\kappa_s}{r_1} \frac{(|\mathbf{r}_{i+1} - \mathbf{r}_i| - r_0)^2}{2} - \frac{\kappa_b}{r_1}(\mathbf{t}_{i+1} \cdot \mathbf{t}_i), \qquad (10)$$

where $\mathbf{r}_i$ is the position of bead i, r_0 the rest length of the springs, r_1 the initial distance between the beads ($r_1 > r_0$ for a chain initially under tension), and $\mathbf{t}_i$ the unit vector tangent to the ith bond. The beads interact with the active particles via a stiff repulsive harmonic potential which prevents the active particles from crossing the flexible chain. As the simple argument above suggests, for a given system size, at large stretching constant κ_s, the wall undergoes small fluctuations around its mean position. As κ_s is decreased, the pressure imbalance around the apices of the filament fluctuations is not compensated anymore, and initial microscopic fluctuations evolve into larger-scale, wavelike features whose initial wavelength is controlled by the bending constant κ_b (see Fig. 4). The initial instability is then observed to slowly coarsen, with an exponent compatible with a $1/3$ power law (Fig. 4). Coarsening in an active system is notoriously difficult to assess [44–46], and a more precise characterization of this phenomenon will be addressed in future works.

It is interesting to consider what the instability predicts for flexible filaments which are not pinned at their extremities. Typical snapshots for increasing filament lengths L_f are shown in Fig. 5 and in supplemental movies. First, the bending rigidity prevents significant modulations of very short filaments, allowing only for slow diffusive motion. As L_f increases beyond the smallest unstable wavelength, the filaments bend, leading to the spontaneous formation of a wedge. The pressure difference on both sides of the filament then propels it forward. This explains the propulsion of "parachute-shaped" filaments observed numerically in Ref. [30]. As the size of the polymer increases further, the parachute shape becomes unstable: A full period of an unstable mode develops, and one observes short-lived spontaneous rotors. Finally, upon increasing L_f beyond the period of the fastest growing mode, the pressure imbalance folds the polymer. This instability thus partly explains the atypical folding of polymers in active baths reported numerically in the literature [26–30]. This transition as the size of the filament increases can be monitored in the diffusivity of its center of mass, which exhibits a sharp peak corresponding to self-propelled wedges (Fig. 5).

Remarkably, our formalism allows us to relate the forces exerted on asymmetric objects, such as the parachute-shaped filaments, to the net flow of active particles around them, a result that goes far beyond the sole cases explored in this Letter. To see this, integrate Eq. (5) over a surface containing an isolated object. This leads to

$$\mathbf{F}^{\text{tot}} = -\mathcal{J}/\mu_t, \qquad (11)$$

where $\mathbf{F}^{\text{tot}} \equiv \int d^2\mathbf{r}\rho\nabla V$ is the total force exerted on the object and $\mathcal{J} \equiv \int d^2\mathbf{r}\mathbf{J}(r)$ the total current of active particles [38]. In the limit of slow, quasistatic motion of the object, Eq. (11) relates in a simple formula the ability of an asymmetric object to act as a ratchet to its self-propulsion by an active bath.

Conclusions.—In summary, we have shown, both analytically and numerically, that, while the forces exerted by an active fluid on a structured wall are, in general, inhomogeneous, an equation of state is recovered upon a proper spatial averaging. This result holds for noninteracting active particles as well as in the presence of pairwise interactions. Walls lacking an "up-down" symmetry act as ratchets and generate transverse fluxes. While the mean force normal to the wall axis still satisfies an equation of state, there is now a wall-dependent shear stress. The numerics shown in this Letter for ABPs are complemented in Ref. [38] by similar

results for RTPs which highlight their generality. For flexible boundaries, we have shown how the fluctuations of the wall shape can be enhanced by pressure inhomogeneities which trigger a modulational instability. For freely moving objects and filaments, this instability sheds new light on a host of phenomena which have been observed numerically, such as the atypical looping and swelling of polymers in active baths [26–30], as well as predicts new behaviors.

This work paves the way to new interesting questions in the engineering and control of active fluids. It would be interesting, for example, to determine how the shear stress generated by walls with asymmetric roughness can be optimized, or whether the dependence of the active motility of semiflexible filaments on their size can be used as a sorting mechanism.

J. T. was supported by ANR project Bactterns. N. N. and Y. K. are supported by an I-CORE Program of the Planning and Budgeting Committee of the Israel Science Foundation and an Israel Science Foundation grant. A. P. S. acknowledges funding through a PLS fellowship from the Gordon and Betty Moore foundation. M. K. is supported by NSF Grant No. DMR-12-06323.

[1] M. C. Marchetti, J. F. Joanny, S. Ramaswamy, T. B. Liverpool, J. Prost, M. Rao, and T. B. Aditi Simha, Rev. Mod. Phys. **85**, 1143 (2013).
[2] F. Julicher, K. Kruse, J. Prost, and J. F. Joanny, Phys. Rep. **449**, 3 (2007).
[3] M. Poujade, E. Grasland-Mongrain, A. Hertzog, J. Jouanneau, P. Chavrier, B. Ladoux, A. Buguin, and P. Silberzan, Proc. Natl. Acad. Sci. U.S.A. **104**, 15988 (2007).
[4] C.-P. Heisenberg and Y. Bellaïche, Cell **153**, 948 (2013).
[5] P. Galajda, J. Keymer, P. Chaikin, and R. Austin, J. Bacteriol. **189**, 8704 (2007).
[6] J. Tailleur and M. Cates, Europhys. Lett. **86**, 60002 (2009).
[7] N. Koumakis, C. Maggi, and R. Di Leonardo, Soft Matter **10**, 5695 (2014).
[8] R. Di Leonardo, L. Angelani, D. DellfArciprete, G. Ruocco, V. Iebba, S. Schippa, M. Conte, F. Mecarini, F. De Angelis, and E. Di Fabrizio, Proc. Natl. Acad. Sci. U.S.A. **107**, 9541 (2010).
[9] A. Sokolov, M. M. Apodaca, B. A. Grzybowski, and I. S. Aranson, Proc. Natl. Acad. Sci. U.S.A. **107**, 969 (2010).
[10] S. A. Mallory, A. Šarić, C. Valeriani, and A. Cacciuto, Phys. Rev. E **89**, 052303 (2014).
[11] X. Yang, M. L. Manning, and M. C. Marchetti, Soft Matter **10**, 6477 (2014).
[12] S. C. Takatori, W. Yan, and J. F. Brady, Phys. Rev. Lett. **113**, 028103 (2014).
[13] A. P. Solon, Y. Fily, A. Baskaran, M. E. Cates, Y. Kafri, M. Kardar, and J. Tailleur, Nat. Phys. **11**, 673 (2015).
[14] F. Smallenburg and H. Löwen, Phys. Rev. E **92**, 032304 (2015).
[15] W. Yan and J. F. Brady, J. Fluid Mech. **785**, R1 (2015).
[16] R. G. Winkler, A. Wysocki, and G. Gompper, Soft Matter **11**, 6680 (2015).
[17] T. Speck and R. L. Jack, Phys. Rev. E **93**, 062605 (2016).
[18] S. C. Takatori and J. F. Brady, Phys. Rev. E **91**, 032117 (2015).
[19] A. P. Solon, J. Stenhammar, R. Wittkowski, M. Kardar, Y. Kafri, M. E. Cates, and J. Tailleur, Phys. Rev. Lett. **114**, 198301 (2015).
[20] J. Elgeti and G. Gompper, Europhys. Lett. **101**, 48003 (2013).
[21] Y. Fily and M. C. Marchetti, Phys. Rev. Lett. **108**, 235702 (2012).
[22] J. Tailleur and M. E. Cates, Phys. Rev. Lett. **100**, 218103 (2008).
[23] M. E. Cates and J. Tailleur, Annu. Rev. Condens. Matter Phys. **6**, 219 (2015).
[24] Y. Fily, A. Baskaran, and M. F. Hagan, Soft Matter **10**, 5609 (2014).
[25] Y. Fily, A. Baskaran, and M. F. Hagan, Phys. Rev. E **91**, 012125 (2015).
[26] A. Kaiser and H. Löwen, J. Chem. Phys. **141**, 044903 (2014).
[27] H.-s. Li, B.-k. Zhang, J. Li, W.-d. Tian, and K. Chen, J. Chem. Phys. **143**, 224903 (2015).
[28] J. Harder, C. Valeriani, and A. Cacciuto, Phys. Rev. E **90**, 062312 (2014).
[29] H. Vandebroek and C. Vanderzande, Phys. Rev. E **92**, 060601 (2015).
[30] J. Shin, A. Cherstvy, W. K. Kim, and R. Metzler, arXiv: 1507.03192.
[31] A. Kaiser, S. Babel, B. ten Hagen, C. von Ferber, and H. Löwen, J. Chem. Phys. **142**, 124905 (2015).
[32] A. Maitra, P. Srivastava, M. Rao, and S. Ramaswamy, Phys. Rev. Lett. **112**, 258101 (2014).
[33] N. Kikuchi, A. Ehrlicher, D. Koch, J. A. Käs, S. Ramaswamy, and M. Rao, Proc. Natl. Acad. Sci. U.S.A. **106**, 19776 (2009).
[34] S. A. Mallory, C. Valeriani, and A. Cacciuto, Phys. Rev. E **92**, 012314 (2015).
[35] In all the numerics, $\mu_t = 1$.
[36] This holds for noninteracting active particles with *macroscopic* wall modulations; its origin lies in the activity of the particles and has nothing to do with the nonuniformity of pressure seen at the microscopic scale for equilibrium interacting particle systems. See J.-P. Hansen and I. R. McDonald, *Theory of Simple Liquids* (Elsevier, New York, 1990).
[37] $P_x(\mathbf{r})$ is the component of the normal force per unit area in the x direction, which for simplicity we denote as "pressure."
[38] See Supplemental Material at http://link.aps.org/supplemental/10.1103/PhysRevLett.117.098001 for full derivations and additional numerical simulations.
[39] G. Falasco, F. Baldovin, K. Kroy, and M. Baiesi, arXiv: 1512.01687.
[40] C. Reichhardt and C. J. Olson Reichhardt, Phys. Rev. E **88**, 062310 (2013).
[41] B.-Q. Ai and J.-C. Wu, J. Chem. Phys. **140**, 094103 (2014).
[42] L. Angelani, A. Costanzo, and R. Di Leonardo, Europhys. Lett. **96**, 68002 (2011).
[43] E. Yariv and O. Schnitzer, Phys. Rev. E **90**, 032115 (2014).
[44] A. G. Thompson, J. Tailleur, M. E. Cates, and R. A. Blythe, J. Stat. Mech. Theor. Exp. (**2011**) P02029.
[45] G. S. Redner, M. F. Hagan, and A. Baskaran, Phys. Rev. Lett. **110**, 055701 (2013).
[46] J. Stenhammar, A. Tiribocchi, R. J. Allen, D. Marenduzzo, and M. E. Cates, Phys. Rev. Lett. **111**, 145702 (2013).